

# Compressive Behavior of Open-Cell Titanium Foams with Different Unit Cell Geometries

Xue-Zheng Yue, Keiji Matsuo and Koichi Kitazono\*

Graduate School of System Design, Tokyo Metropolitan University, Tokyo 191-0065, Japan

Mechanical properties of open-cell titanium foams with different cell geometries (truncated octahedron and rhombic dodecahedron cells) were examined through compressive tests. These foams were manufactured through the electron beam melting (EBM) process. The compressive behavior depends on the porosity, cell geometry and the cell orientation. Titanium foams with truncated octahedron cells showed high strength compared to those of rhombic dodecahedron cells. This is due to the short cell edges in truncated octahedron cells. In addition, the parallel and oblique cell edges against the compression direction are effective to increase the compressive strength. Macroscopic shear bands caused by ordered cell geometry were observed in some titanium foams. [doi:10.2320/matertrans.L-M2017834]

(Received May 30, 2017; Accepted August 8, 2017; Published October 25, 2017)

**Keywords:** titanium foam, electron beam melting, truncated octahedron, rhombic dodecahedron

## 1. Introduction

Metal foams are a class of lightweight materials with novel physical, mechanical, thermal, electrical and acoustic properties. They offer potential for lightweight structures, energy absorption, and thermal management<sup>1</sup>. Titanium foams are used for structural applications or for bone-replacement implants because of their low density, high strength and excellent corrosion resistance<sup>2,3</sup>.

Powder metallurgical (PM) process with spacer materials has been used for the manufacturing of magnesium<sup>4,5</sup> and titanium<sup>6,7</sup> foams. Due to the non-spherical shape of the spacer materials, the cell structure of metal foams becomes homogeneous, and the pore shape becomes heterogeneous. Recently, additive manufacturing (AM) technology has been focused on many industrial applications<sup>8</sup>. In the case of metallic parts, selective electron beam melting (EBM)<sup>9</sup>, selective laser sintering (SLS)<sup>10</sup> and selective laser melting (SLM)<sup>11-13</sup> have enabled to produce highly porous interconnected structures. The arbitrary pore shapes and pore sizes are in the range from 100 to 200  $\mu\text{m}$ , which can create complex and ordered structure titanium foam that is distinguished from previous approaches<sup>14,15</sup>.

AM process enables to manufacture open-cell geometry consisting of periodic space-filling polyhedrons. Though there are several space-filling polyhedrons, the present study focusses on two polyhedrons, truncated octahedron and rhombic dodecahedron. A truncated octahedron, which is one of Archimedean solids, has 14 faces (8 hexagons and 6 squares), 36 edges and 24 vertices. A rhombic dodecahedron, which is one of Catalan solids, has 12 rhombic faces, 24 edges and 14 vertices. Of course, titanium foams with these polyhedron cell geometries have been reported in the previous study<sup>16</sup>. However, the relationship between the porosity, cell edge length, cell diameter and cell orientation has not been discussed systematically.

In the present study, mechanical properties of titanium foams with truncated octahedron and rhombic dodecahedron cells are investigated systematically. Optimal cell geometry

for mechanical properties such as plateau stress and energy absorption is clarified through the compressive tests.

## 2. Experimental Procedure

Periodic truncated octahedron and rhombic dodecahedron open-cell geometries are constructed by using a commercial 3D-CAD software. 3D images of the unit-cells are shown in Fig. 1. Octa\_A and Octa\_B are the truncated octahedron cells with the edge length of  $a$ . In the  $x$ - $y$ - $z$  orthogonal coordinate system, Octa\_B has cell geometry after 54.7 deg rotation around  $y$ -axis and 45 deg rotation around  $z$ -axis of Octa\_A. Dodeca\_A, Dodeca\_B and Dodeca\_C are the rhombic dodecahedron cells with the edge length of  $a$ . In the  $x$ - $y$ - $z$  orthogonal coordinate system, Dodeca\_B has cell geometry after 90 deg rotation around  $x$ -axis of Dodeca\_A. Dodeca\_C has cell geometry after 54.7 deg rotation around  $y$ -axis of Dodeca\_A. Here, the compression direction is parallel to  $z$ -axis.

In the case of truncated octahedron unit cell with the edge length,  $a$ , the volume is expressed as

$$V_0^{\text{Octa}} = 8\sqrt{2}a^3. \quad (1)$$

By assuming the cylindrical shape of the cell edges, the volume of cell edges in the unit cell is calculated as

$$V_a^{\text{Octa}} = \frac{\pi}{4}t^2 \times \frac{1}{3} \times a \times 36 = 3\pi at^2 \quad (2)$$

where  $t$  is the diameter of cylindrical edges. Therefore, the nominal porosity,  $p_N$ , becomes

$$p_N^{\text{Octa}} = \frac{V_0^{\text{Octa}} - V_a^{\text{Octa}}}{V_0^{\text{Octa}}} = 1 - \frac{3\sqrt{2}\pi}{16} \left(\frac{a}{t}\right)^{-2}. \quad (3)$$

In the case of rhombic dodecahedron unit cell with the edge length,  $a$ , the volume is expressed as

$$V_0^{\text{Dodeca}} = \frac{16}{9}\sqrt{3}a^3. \quad (4)$$

By assuming the cylindrical shape of the cell edges, the volume of cell edges in the unit cell is calculated as

\*Corresponding author, E-mail: kitazono@tmu.ac.jp

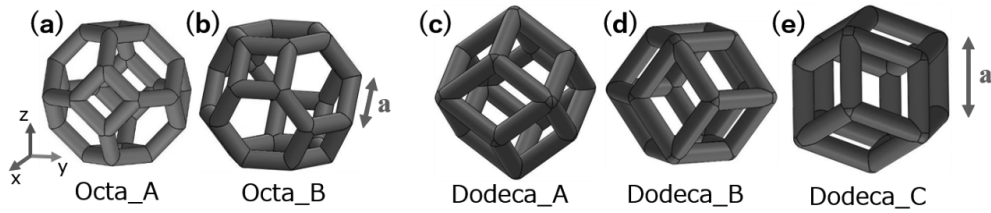


Fig. 1 3D-CAD images of two types of truncated octahedron unit cells, (a) and (b), and three types of rhombic dodecahedron unit cells, (c), (d) and (e). Compression direction is parallel to the z-axis.

$$V_a^{\text{Dodeca}} = \frac{\pi}{4} t^2 \times \frac{1}{3} \times a \times 24 = 2\pi a t^2 \quad (5)$$

where  $t$  is the diameter of cylindrical edges. Therefore, the nominal porosity becomes

$$p_N^{\text{Dodeca}} = \frac{V_0^{\text{Dodeca}} - V_a^{\text{Dodeca}}}{V_0^{\text{Dodeca}}} = 1 - \frac{3\sqrt{3}\pi}{8} \left(\frac{a}{t}\right)^{-2} \quad (6)$$

The nominal porosities of both truncated octahedron cell and rhombic dodecahedron cell are plotted as a function of the normalized edge length in Fig. 2(a). The normalized porosity increases with increasing the normalized edge length. The edge length of the rhombic dodecahedron unit cell is longer than that of the truncated octahedron unit cell.

When the volume of the unit cell is equivalent to the volume of sphere with the diameter of  $d$ , each nominal porosity is expressed as

$$p_N^{\text{Octa}} = 1 - 3^{\frac{5}{3}} \times 2^{-\frac{1}{2}} \times \pi^{\frac{1}{3}} \times \left(\frac{d}{t}\right)^{-2} \quad (7)$$

$$p_N^{\text{Dodeca}} = 1 - 3^{\frac{7}{6}} \times (2\pi)^{\frac{1}{3}} \times \left(\frac{d}{t}\right)^{-2} \quad (8)$$

The nominal porosities are plotted as a function of the normalized cell diameter in Fig. 2(b). Relationship between the normalized porosity and normalized cell diameter of two unit cells becomes almost the same. The nominal porosities of the present titanium foam specimens are 80% and 90%. Since the thickness of all cell edges are fixed at 1 mm, the cell diameters of specimens with 80% and 90% porosities are about 6 mm and 8 mm, respectively.

Open-cell titanium foams with different porosities and cell geometries were manufactured in vacuum through 3D EBM process. Arcam A2X machine designed for titanium alloys was used in this study. Commercially pure titanium, Grade 2, powder was used as a starting material. The chemical composition is shown in Table 1. The shape of the compressive specimens have cylindrical shape with 30 mm in diameter and 30 mm in height. Building direction was parallel to the cylindrical axis. No heat treatment was carried out after EBM process. Mechanical properties of the titanium foam specimens were examined by compressive tests at room temperature using a Shimadzu Autograph AG-50kNISD. Crosshead speed was fixed at 10 mm/min.

### 3. Results

#### 3.1 Effect of porosity

Photographs of cylindrical titanium foam specimens are

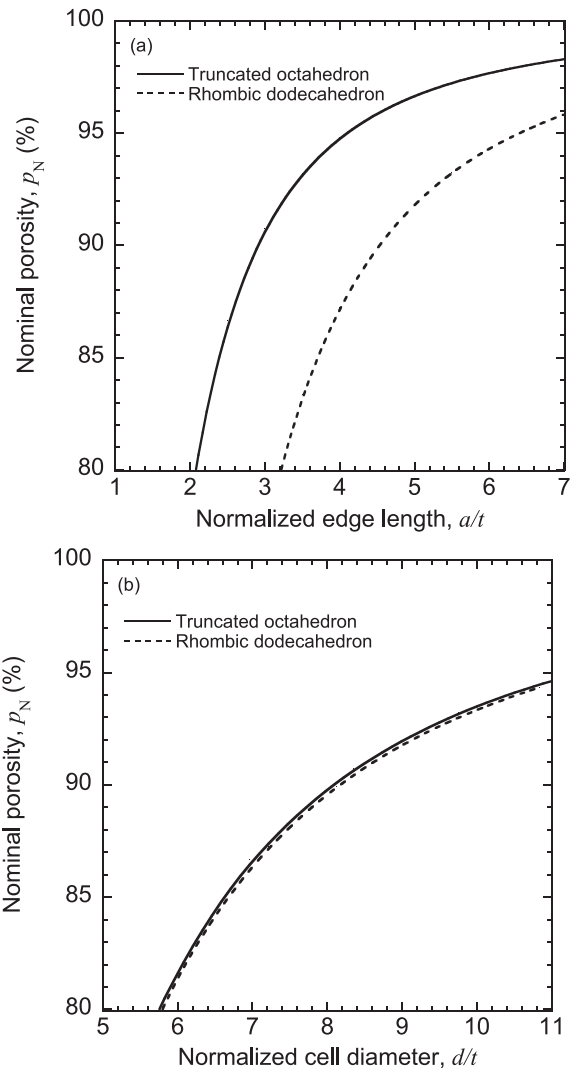


Fig. 2 Nominal porosities of truncated octahedron and rhombic dodecahedron unit cells are plotted as a function of (a) the normalized edge length and (b) the normalized cell diameter.

Table 1 Chemical composition of commercially pure titanium, Grade 2, powder.

Element	C	Fe	O	N	H	Ti
mass%	0.02–0.08	0.07–0.3	0.14–0.25	0.02–0.03	0.002–0.015	Bal

shown in Fig. 3. Vertical direction is parallel to the compression direction. Thickness of the cell edge is 1 mm in all specimens. It is noted that the cell diameters of truncated oc-

tahedron unit cells are the same as those of rhombic dodecahedron cells at the same porosity.

Compressive stress-strain curves of ten kinds of titanium foam specimens are shown in Fig. 4. The plateau stresses of Octa\_A (80% and 90%) are 28.9 MPa and 7.4 MPa, respectively. The plateau stresses of Octa\_B (80% and 90%) are 18.4 MPa and 5.3 MPa, respectively. The plateau stresses of Dodeca\_A (80% and 90%) are 17.9 MPa and 4.7 MPa, respectively. The plateau stresses of Dodeca\_B (80% and 90%) are 17.3 MPa and 3.7 MPa, respectively. The plateau stresses of Dodeca\_C (80% and 90%) are 23.9 MPa and 5.4 MPa, respectively. Yield stress of dense Grade 2 titanium manufactured through 3D EBM process has been reported as 540 MPa, which was much higher than those of the present titanium foams. The absorbed energy up to 50% strain of Octa\_A (80% and 90%) are 6.5 MJ/m<sup>3</sup> and 2.2 MJ/m<sup>3</sup>, respectively. The absorbed energy of Octa\_B (80% and 90%) are 4.1 MJ/m<sup>3</sup> and 1.6 MJ/m<sup>3</sup>, respectively. The absorbed energy of Dodeca\_A (80% and 90%) are 4.1 MJ/m<sup>3</sup> and 1.3 MJ/m<sup>3</sup>, respectively. The absorbed energy of Dodeca\_B (80% and 90%) are 4.1 MJ/m<sup>3</sup> and 1.2 MJ/m<sup>3</sup>, respectively. The absorbed energy of Dodeca\_C (80% and 90%) are 5.9 MJ/m<sup>3</sup> and 1.8 MJ/m<sup>3</sup>, respectively. Both the plateau stress and absorbed energy of titanium foams with 80% porosity were higher than those of 90% porosity.

### 3.2 Effect of shape of unit cell

The plateau stresses of truncated octahedron cells were higher than those of rhombic dodecahedron cells. Energy absorption of truncated octahedron cells were also higher than those of rhombic dodecahedron cells. As shown in Fig. 2(b), the cell diameter of these cells are the same. Therefore, the difference is not due to the size effect.

### 3.3 Effect of compression direction

The plateau stress and the absorbed energy of Octa\_A specimen were higher than those of Octa\_B specimen. The plateau stress and the absorbed energy of Dodeca\_C specimen were higher than those of Dodeca\_A and Dodeca\_B specimens. The plateau stress and the absorbed energy of

Dodeca\_A and Dodeca\_B are almost the same. These differences were caused by the anisotropic deformation of open-cell titanium foams.

### 3.4 Macroscopic shear bands

Photographs of the titanium foam specimens at the compressive strain of 20% are shown in Fig. 5. Octa\_A and Dodeca\_A specimens showed relatively uniform deformation. On the other hand, the macroscopic shear bands are observed in Octa\_B, Dodeca\_B and Dodeca\_C specimens. Oscillations of the stress-strain curves observed in these specimens [Fig. 4 (b), (d) and (e)] are due to the shear band formation.

## 4. Discussion

Mechanical properties of the present titanium foam specimens are listed in Table 2. In many metal foams, the relationship between the plateau stress and the relative density has been expressed by

$$\sigma_P = C\sigma_S \left( \frac{\rho^*}{\rho_S} \right)^n \quad (9)$$

where  $C$  is the constant,  $\sigma_S$  is the yield stress of the cell wall material,  $\rho^*$  is the density of the foam,  $\rho_S$  is the density of the cell wall material and  $n$  is the density exponent. In the present open-cell titanium foams, the value of  $n$  is almost equal to two, which is independent of the cell geometry. If the metal foam has completely plateau region, the relationship between the absorbed energy and the relative density becomes identical to that of plateau stress. However, the value of  $n$  in energy absorption was slightly smaller than that of plateau stress. This is due to the oscillation of compressive stress-strain curves caused by the formation of macroscopic shear bands.

The strength of the present titanium foams depended on the cell geometry. Titanium foams with truncated octahedron cells showed higher strength than those with rhombic dodecahedron cells. This is due to the cell edge length. In the case of open-cell metal foams, the main mechanism of com-

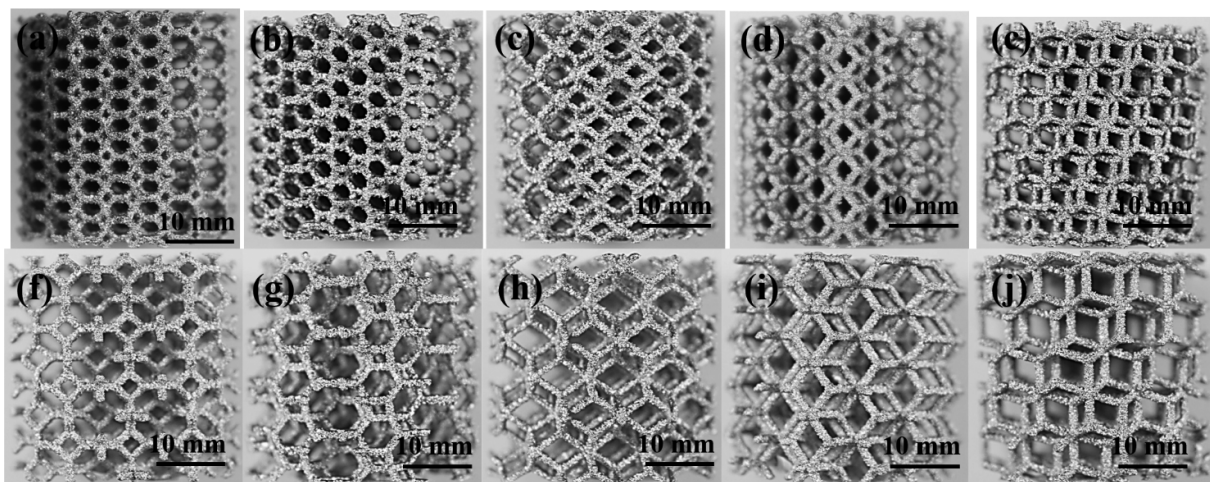


Fig. 3 Photographs of open-cell titanium foam specimens manufactured through EBM process. Octa\_A (a,b), Octa\_B (b,g), Dodeca\_A (c,h), Dodeca\_B (d,i), Dodeca\_C (e,j). Each nominal porosity is 80% (a-e) and 90% (f-j).

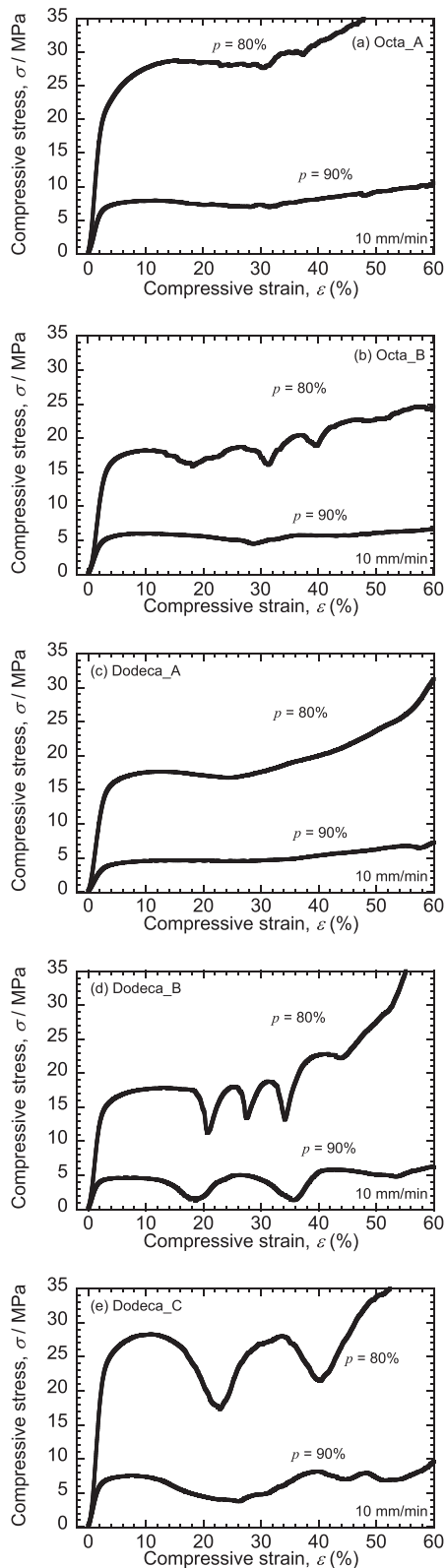


Fig. 4 Compressive stress-strain curves of open-cell titanium foams, (a) Octa\_A, (b) Octa\_B, (c) Dodeca\_A, (d) Dodeca\_B and (e) Dodeca\_C with different porosities. The crosshead speed is fixed at 10 mm/min.

pressive deformation is the bending or buckling of the cell edges. According to the simple beam theory, the short beams shows high resistance to bending or buckling. As shown in Fig. 2(a), the cell edge length of the truncated octahedron cells is shorter than that of rhombic dodecahedron cells.

Therefore, we can conclude that the truncated octahedron cell geometry is effective to increase the strength compared to the rhombic dodecahedron cell geometry.

The strength of the present titanium foams also depended on the compression direction. This is due to the orientation of the cell edges. Orientation of the cell edges are classified to three types: parallel, perpendicular and oblique cell edges against the compression direction ( $z$ -axis). These cell edges are illustrated as light gray, black and dark gray colors in Fig. 6. The difference between Octa\_A and Octa\_B specimens is due to the number of oblique edges, 24 oblique edges in Octa\_A and 18 oblique edges in Octa\_B [Table 2]. Oblique cell edges have high resistance to the compressive deformation compared to perpendicular cell edges. Therefore, Octa\_A specimen consisting of many oblique cell edges showed high compressive strength compared to Octa\_B specimen. On the other hand, Dodeca\_C specimen has 6 parallel edges, which have highest resistance to compressive deformation. Therefore, Dodeca\_C specimen showed the highest compressive strength compared to Dodeca\_A and Dodeca\_B specimens, which have no parallel edges. The difference between Dodeca\_A and Dodeca\_B specimens is due to the same reason as octahedron specimens. Dodeca\_A specimen consisting of many oblique edges, 24 oblique edges, showed high compressive strength compared to Dodeca\_B specimen consisting of 12 oblique edges.

Present experimental results revealed that the cell geometry of Octa\_A lattice was effective to increase the compressive strength and the absorbed energy. This result can be not only valid for titanium foams but also for other metal foams.

The formation of shear bands can be discussed. At initial period of linear elasticity, no shear band was formed. After the yielding, the shear band generated in the direction of the maximum shear stress of the cylindrical specimen. In the case of conventional metal foams such as ALPORAS aluminum foams, local deformation region like shear band generates in the perpendicular plane against the compression direction. The difference in the compressive deformation is probably due to two reasons. One is the ordered and homogeneous cell geometry in the present 3D EBM titanium foams. In the case of PM titanium foams with disordered cell geometry, no shear band formation has been observed<sup>15)</sup>. Present cell geometry is similar to the bulk single crystal. Therefore, the shear band during the compression was formed in the direction of maximum shear stress. Another is the high buckling strength of the present titanium foams. Modulus and strength of titanium are higher than aluminum. Therefore, the local buckling was limited and the shear band was formed. It is recommended that the soft cell wall materials are effective to reduce the shear band formation. On the other hand, the shear band formation was limited in the titanium foams with 90% porosity against 80% porosity. In the case of high porosity, the local buckling occurred preferentially because of long cell edges.

## 5. Conclusions

Open-cell titanium foams with different porosities and unit cell geometries were manufactured through 3D EBM

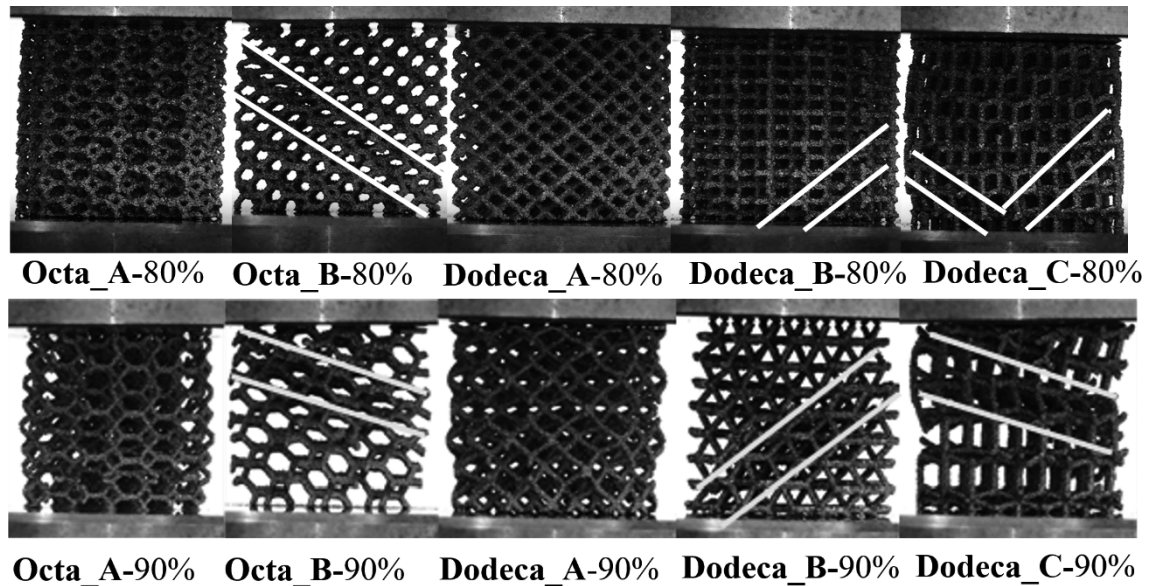


Fig. 5 Photographs of the compressive test specimens at the compressive strain of 20%. Macroscopic shear bands are observed in Octa\_B, Dodeca\_B and Dodeca\_C specimens.

Table 2 Cell geometries and mechanical properties in ten titanium foam specimens are summarized.

Unit cell	Number of			Nominal Porosity, $p_N$ (%)	Cell diameter, $d/t$	Plateau stress, $\sigma_P$ /MPa	Energy absorption, $W/MJm^{-3}$
	Parallel edges	Perpendicular edges	Oblique edges				
Octa_A	0	12	24	80	5.7	28.9	6.5
				90	8.0	7.4	2.2
Octa_B	0	18	18	80	5.7	18.4	4.1
				90	8.0	5.3	1.6
Dodeca_A	0	0	24	80	5.8	17.9	4.1
				90	8.2	4.7	1.3
Dodeca_B	0	12	12	80	5.8	17.3	4.1
				90	8.2	3.7	1.2
Dodeca_C	6	0	18	80	5.8	23.9	5.9
				90	8.2	5.4	1.8

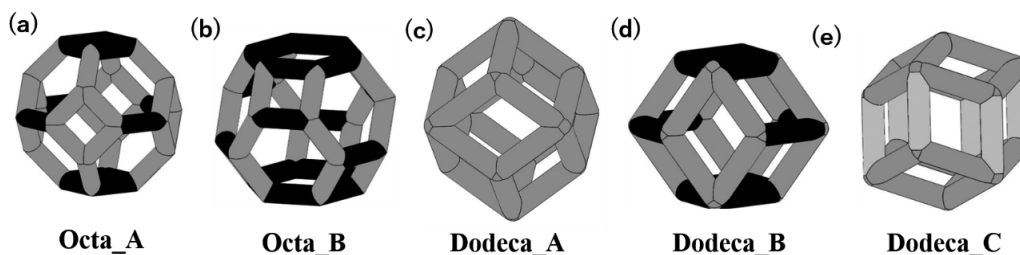


Fig. 6 Parallel, perpendicular and oblique cell edges against the compression direction are colored by light gray, black and dark gray, respectively. (a) Octa\_A, (b) Octa\_B and (d) Dodeca\_B consist of perpendicular and oblique cell edges. (c) Dodeca\_A consists of only oblique cell edges. (e) Dodeca\_C consists of parallel and oblique cell edges.

process. Compressive tests at room temperature achieved the following experimental results.

- (1) Plateau stress and absorbed energy of open-cell titanium foams increased with decreasing the porosity.
- (2) Plateau stress and absorbed energy of the titanium foams with the truncated octahedron unit cells were higher than those of the titanium foams with rhombic

dodecahedron unit cells. This is due to the short cell edges in truncated octahedron unit cells compared to in rhombic dodecahedron cells.

- (3) Plateau stresses of Octa\_A and Dodeca\_C specimens were higher than those of other specimens. The reason is due to the orientation of the cell edges. Parallel edges against the compression direction are effective to in-

crease the initial flow stress.

(4) Metal foams consisting of Octa\_A lattice have a potential for energy absorbing applications.

In addition, the macroscopic shear bands were formed in some specimens. It caused the decrease in the absorbed energy. Mechanism of the shear band formation can be explained by both the ordered cell geometry and the buckling strength of the base material. Disordered cell geometry and soft material are probably effective to reduce the shear band formation. These result are not only valid for the present titanium foams but also for other metal foams such as aluminum foams.

### Acknowledgements

This work was financially supported in part by Advisory Committee for Space Engineering, Japan Aerospace Exploration Agency, and The Light Metal Educational Foundation, Japan.

### REFERENCES

- 1) M. F. Ashby, A. Evans, N. A. Fleck, L. J. Gibson, J. W. Hutchinson, H. N. G. Wadley: *Metal Foams: A Design Guide*, (Butterworth-Heinemann, Boston, 2000) 33–34.
- 2) X. Jian, C. Hao, Q. Guibao, Y. Yang and L. Xuewei: *Mater. Des.* **88** (2015) 132–137.
- 3) G. Kotan and A.Ş. Bor: *Turkish J. Eng. Env. Sci.* **31** (2007) 149–156.
- 4) X. Yue and B.Y. Hur: *Kor. J. Mater. Res.* **22** (2012) 309–315.
- 5) X. Yue and B.Y. Hur: *J. Korean Found. Soc.* **32** (2012) 150–156.
- 6) N.G.D. Murray and D.C. Dunand: *Compos. Sci. Technol.* **63** (2003) 2311–2316.
- 7) X. Yue, K. Kitazono, X. Yue and B.Y. Hur: *J. Mag. Alloys* **4** (2016) 1–7.
- 8) Y. Jiang and Q. Wang: *Sci. Rep.* **6** (2016) 34147.
- 9) P. Heinl, C. Körner and R.F. Singer: *Adv. Eng. Mater.* **10** (2008) 882–888.
- 10) T. Traini, C. Mangano, R.L. Sammons, F. Mangano, A. Macchi and A. Piattelli: *Dent. Mater.* **24** (2008) 1525–1533.
- 11) L. Mullen, R.C. Stamp, W.K. Brooks, E. Jones and C.J. Sutcliffe: *J. Biomed. Mater. Res. B Appl. Biomater.* **89** (2009) 325–334.
- 12) M. Salmi, K. Paloheimo, J. Tuomi, J. Wolff and A. Mäkitie: *J. Craniofac. Surg.* **41** (2013) 603–609.
- 13) X.-B. Su, Y.-Q. Y., P. Yu and J.-F. S.: *Trans. Nonferrous Met. Soc. China* **22** (2012) s181–s187.
- 14) L.E. Murr, E.V. Esquivel, S.A. Quinones, S.M. Gaytan, M.I. Lopez, E.Y. Martinez, F. Medina, D.H. Hernandez, E. Martinez, J.L. Martinez, S.W. Stafford, D.K. Brown, T. Hoppe, W. Meyers, U. Lindhe and R.B. Wicker: *Mater. Character.* **60** (2009) 96–105.
- 15) X. Yue, H. Fukazawa and K. Kitazono: *Mater. Sci. Eng. A* **673** (2016) 83–89.
- 16) L. Xiao, W. Song, C. Wang, H. Liu, H. Tang and J. Wang: *Mater. Sci. Eng. A* **640** (2015) 375–384.